



## OPEN A study on the cellular adhesion properties of a hybrid scaffold for vascular tissue engineering through molecular dynamics simulation

Faeze Shams<sup>1,2</sup>, Mostafa Jamshidian<sup>1</sup>, Hossein Shaygani<sup>1,2</sup>, Sasan Maleki<sup>1</sup>,  
Mohamadreza Soltani<sup>1,2</sup> & Amir Shamloo<sup>1,2</sup>✉

Utilizing biocompatible hybrid scaffolds that promote cell adhesion and proliferation is critically significant in the field of tissue engineering. In order to achieve this goal, the composition of polymers in the sample should be adjusted accordingly. In this research, molecular dynamics simulations are utilized to investigate how the composition of blends influences the protein adsorption properties of hybrid scaffolds. Scaffolds considered here consist of Bombyx mori silk fibroin (B. mori SF) and thermoplastic polyurethane (TPU) intended for application in vascular grafts. Three different compositions are investigated in this study: One sample with 70% TPU by volume (SF:TPU-3/7), the second sample with 50% TPU (SF:TPU-1/1) and the last sample with 30% TPU (SF:TPU-7/3). The interaction between the polymeric scaffold surfaces and fibronectin and laminin, two major proteins found in vascular tissues, is studied using molecular dynamics simulations. The biocompatibility of each sample is examined based on calculated adhesion energy and final protein conformation. Furthermore, MTT cell viability, cell adhesion, and live/dead assays are performed to validate the simulation results. Third-passage human umbilical vein cell (HUVEC) is utilized in this study. The simulations revealed that B. mori SF (SF) content in the blend needs to be balanced with TPU to enhance the protein adsorption strength. The experimental results exhibited a correlation with the simulations and were verified with cell adhesion and staining assays. The SF:TPU-1/1 had the highest cell viability followed by SF:TPU-7/3 and SF:TPU-3/7 with ~ 94.7%, ~ 85.5%, and ~ 78.9%, respectively, demonstrating the accuracy of the simulations and the possibility of predicting the biocompatibility of biomaterials through simulations.

**Keywords** Tissue engineering, Hybrid scaffold, Protein adsorption, Molecular dynamics simulations, Adhesion energy, Vascular graft

In recent years, there has been a growing interest in the utilization of composite (hybrid) biocompatible scaffolds for applications in tissue engineering. Combining biomaterials with different physical and chemical properties is the key idea to achieving the desired characteristics. Providing a biocompatible scaffold with optimum cell adhesion and proliferation is an essential demand in this field. To achieve this aim, various synthetic and natural polymers, exhibiting either hydrophilic or hydrophobic characteristics, with distinct compositions are combined<sup>1,2</sup>. The composition of the polymers in the blend is a key parameter that allows us to modify the properties of the scaffold<sup>2,3</sup>. In order to create a well-defined structure that promotes optimal cell attachment, it is essential to identify the suitable composition of the blend. Determining the optimal ratio of polymers within a sample presents the main challenge in the development of an ideal scaffold. Conducting experimental assays represents one potential method for investigating how the composition of blends influences the biocompatibility and cell adhesion properties of the scaffold. This approach is both time-consuming and expensive because fabrication and experimental assays must be repeated for every possible structure. Computational tools represent an alternative method for assessing the biocompatibility of suggested blends. The results of the simulations can be considered as an estimation of the cell adhesion capability of different blends and help us to get closer to the optimum composition. A limited number of proposed compositions that exhibit acceptable biocompatibility

<sup>1</sup>Nano-Bioengineering laboratory, Department of Mechanical Engineering, Sharif University of Technology, Tehran 11365-11155, Iran. <sup>2</sup>Stem Cell and Regenerative Medicine Center, Sharif University of Technology, Tehran 11365-11155, Iran. ✉email: shamloo@sharif.edu

have been identified based on the simulation results. Experimental assays are being performed on this group to identify the most effective composition.

Earlier research indicate a significant correlation between the properties of cell adhesion and the selective adsorption of ECM proteins onto the surface of the scaffold. This is because ECM proteins play a critical role in cell attachment within tissues in the body<sup>4,5</sup>. A strong and reliable computational tool for studying protein adsorption on a designated surface enables us to approximate the biocompatibility of the proposed scaffold. This process involves enhancing the cell adhesion potential of the structure.

Molecular dynamics simulation is a powerful computational tool for modelling atomistic interactions at the nanoscale. This technique can be utilized in the field of biotechnology for studying the interaction among different biomolecules, macromolecules and other biological processes. A number of researchers have adopted this approach to investigate the interaction between proteins and structured surfaces. Raffaini and Ganazzoli<sup>6</sup> utilized atomistic computer simulations to investigate the interaction of some albumin subdomains with a flat hydrophobic graphite surface. They claimed that their proposed adsorption mechanism was consistent with experimental results. Heidari and Shamloo<sup>7</sup> examined how surface roughness influences the adhesive properties of graphene sheets. They considered adhesion energy and peeling force as two main criteria for adhesion. In accordance with simulation results, they found that an increase in surface roughness leads to rise in adhesion energy and thereby enhancing the stability of the system.

Some other published studies have focused on the adsorption of proteins onto polymeric and amorphous surfaces. Regis et al.<sup>8</sup> utilized experimental methods and molecular dynamic simulations to investigate the adsorption of fibronectin onto functionalized electrospun PCL scaffolds. They conducted an experimental quantification of the fluorescently labeled absorption across three groups of scaffolds and discovered that the laminated PCL scaffold exhibits a higher adsorption of fibronectin compared to the untreated scaffold. Additionally, they found that hydrolysis of the scaffold's surface resulted in a reduction of fibronectin adsorption. According to this study, molecular dynamics simulations can predict the ultimate conformation of proteins, which significantly influences subsequent cell adhesion. Sarmadi et al.<sup>1</sup> employed molecular dynamics simulations in conjunction with experimental methods to optimize the biocompatibility of a hybrid scaffold. A simulation was performed to investigate the adsorption of collagen type I and fibronectin onto six distinct blends of PCL and PVA. The adhesion energy and ultimate protein conformation of samples containing over 50% PCL showed a favorable environment for the adsorption of ECM proteins. In this study, MTT assays indicated that samples containing a higher hydrophobic component exhibited improved initial cell attachment and proliferation, consistent with the simulation results. In all the above studies, protein adhesion energy has been considered as an essential parameter for examining cell attachment strength to the surface. In a general sense, the ultimate conformation of proteins<sup>9</sup>, including their size and hydrophobic characteristics<sup>6</sup>, as well as surface properties such as hydrophobicity and functionalization<sup>10–12</sup> are essential factors that influence how proteins interact with surfaces.

In this research, a hybrid scaffold integrating both natural and synthetic polymers has been developed to address the limitations associated with single-polymer scaffolds and to tailor the structural properties for particular applications. Molecular dynamics simulations are utilized to examine the adhesion of some vital Extracellular Matrix (ECM) proteins on polymeric surfaces. By using this approach, different scaffolds that replace damaged organs and tissues can be assessed for biocompatibility. In order to build vascular graft scaffolds, thermoplastic polyurethane (TPU) is combined with Bombyx mori silk fibroin (B. mori SF). TPU is a synthetic biodegradable and cytocompatible polymer with superior mechanical properties and blood compatibility. The excellent elasticity and durability of this polymer make it ideal for enduring the dynamic environment inside blood vessels. Meanwhile, TPU exhibits biocompatibility and interacts favorably with blood components<sup>13–16</sup>. B. mori SF (SF) is a natural polymer with exceptional biocompatibility and controlled biodegradability, supporting tissue integration and cell adhesion. According to the research conducted by Tungtasana et al., the biodegradation of scaffolds made from Bombyx mori Thai silk fibroin was examined both in vitro and in vivo. The in vivo studies revealed that all scaffolds remained detectable even after 12 weeks of implantation in the subcutaneous tissue of Wistar rats<sup>17</sup>. In vitro test results showed that more than 50% mass loss occurred within 28 days for a scaffold made from SF<sup>17</sup>. Due to its high tensile strength, SF augments the scaffold's structural integrity. Moreover, the hemocompatibility of SF can be enhanced through surface modifications to improve its interactions with blood components<sup>16,18–20</sup>. Through the combination of TPU and SF, we can create scaffolds with enhanced mechanical properties, improved biocompatibility, and controlled biodegradability, mimicking the natural extracellular matrix of blood vessels<sup>15</sup>. Three compositions of SF:TPU-3/7, SF:TPU-1/1, and SF:TPU-7/3 are examined in this study. The percentages were chosen to encompass a variety of different characteristics like hydrophobicity that could be correlated with biocompatibility through experimental and computational approaches<sup>21</sup>. All simulations are performed in Material Studio software (v. 2017). Two abundant ECM proteins related to endothelial cells viability, including fibronectin and laminin<sup>22</sup> are considered to study their interaction with different polymeric surfaces based on adhesion energy and final protein conformation. In the experimental section cell proliferation on electrospun scaffolds is studied using MTT assays. Third-passage human umbilical vein cells (HUVEC) are used in all experiments. A good quantitative estimate of the number of cells adhered to a scaffold surface can be obtained using MTT results<sup>23,24</sup>. In order to investigate cell attachment more precisely, SEM images are exploited as a qualitative tool in this study. Live/dead assays are also conducted to study cell attachment and viability qualitatively.

## Materials and methods

### Molecular dynamics simulation

#### Governing equations

In this research, the Material Studio software (v. 2017) is employed to simulate the interaction between proteins and polymeric surfaces. The Dreiding force field is applied in all simulations to compute the potential energy of the system. This force field is widely used for atomic-level simulations of proteins and different polymers. The Dreiding model considers both bonded ( $U_{val}$ ) and non-bonded ( $U_{nb}$ ) energy contributions, as detailed below<sup>25</sup>.

$$U = U_{val} + U_{nb} \quad (1)$$

The energy related to bonding or valence depends on the specific bonds in the structure and consists of four terms: bond stretching ( $U_r$ , two-body), bond-angle bending ( $U_\theta$ , three-body), dihedral angle torsion ( $U_\varphi$ , four-body), and inversion ( $U_\psi$ , four-body) terms.

$$U_{val} = U_r + U_\theta + U_\varphi + U_\psi \quad (2)$$

The non-bonded contribution consists of the terms related to van der Waals interactions ( $U_{vdw}$ ), electrostatic forces ( $U_Q$ ), and hydrogen bonding ( $U_{hb}$ ).

$$U_{nb} = U_{vdw} + U_Q + U_{hb} \quad (3)$$

The Van der Waals term represents the interaction between atoms and molecules that is dependent on short-range distances. This interaction is quantified using the Lennard–Jones potential equation, which is expressed as follows.

$$U_{vdw} = 4\varepsilon_{ij} \left[ \left( \frac{\sigma_{ij}}{r_{ij}} \right)^{12} - \left( \frac{\sigma_{ij}}{r_{ij}} \right)^6 \right] (r_{ij} < r_{cut}) \quad (4)$$

where  $r_{ij}$  represents the separation distance,  $\varepsilon_{ij}$  indicates the equilibrium energy,  $\sigma_{ij}$  refers to the equilibrium distance between the  $i$ th and  $j$ th atoms, and  $r_{cut}$  denotes the cut-off distance, beyond which the van der Waals interactions become negligible. The calculation of electrostatic energy is calculated as follows.

$$U_{vdw} = \frac{q_i q_j}{\varepsilon_{eff} r_{ij}} \quad (5)$$

where  $q_i$  and  $q_j$  represent the atomic charges associated with the  $i$ th and  $j$ th atoms, respectively. The variable  $r_{ij}$  indicates the distance separating the two atoms, while  $\varepsilon_{eff}$  denotes the effective dielectric constant. The expression for the hydrogen bond term is expressed as follows.

$$U_{hb} = D_{hb} \left[ 5 \left( \frac{R_{hb}}{R_{DA}} \right)^{12} - 6 \left( \frac{R_{hb}}{R_{DA}} \right)^{10} \right] \cos^4 \theta_{DHA} \quad (6)$$

$D_{hb}$  and  $R_{hb}$  refer to the hydrogen bond constants referenced in<sup>25</sup>, while  $R_{DA}$  represents the distance separating the hydrogen donor (D) from the hydrogen acceptor (A) atoms. Additionally,  $\theta_{DHA}$  denotes the bond angle formed by hydrogen donor, the hydrogen (H), and the hydrogen acceptor.

### Modeling scaffold structures

The structural components of the polymeric scaffold discussed in this study consist of thermoplastic polyurethane (TPU) and Bombyx mori silk fibroin (B. mori SF). As the simulations are primarily aimed at modeling the interactions between ECM proteins and hybrid scaffolds, all simulations are performed at the protein scale, not the cellular scale, and oligomers rather than fibers are considered in the simulation cells. Therefore, the alignment of the fibers and thickness variation are not taken into account in the simulations<sup>1,8</sup>. In this context, thermoplastic polyurethane is defined as an oligomer comprising 10 repeating units (represented in Fig. 1). Previous studies suggest that the solubility parameter of TPU remains unchanged for oligomers containing more than 9 monomers. Therefore, it is considered appropriate to use oligomers with 10 repeating units in MD simulations<sup>26</sup>. Due to the high computational cost associated with the comprehensive atomistic model of B. mori SF, a simplified model derived from earlier research is utilized in this context. Earlier studies have shown that the fibroin heavy chain is mainly made up of repetitive GAGAGS amino acid sequences. This primary structure possesses the capability to fold into 3  $\beta$ -sheets, with each  $\beta$ -sheet comprising 5 anti-parallel  $\beta$ -strands<sup>27,28</sup>. The secondary structure of this protein is considered here to ensure accuracy. For modelling this structure, the file 1slk.pdb was obtained from the Protein Data Bank, and the terminal residue of each strand was modified from alanine (A) to serine (S) using the mutation plugin in VMD 1.9.3 software. This procedure is necessary for obtaining the GAGAGS sequence<sup>29</sup>. The final coordinate file is then imported into Material Studio software to support the subsequent simulation steps (Fig. 2). After constructing the TPU and SF structures, a geometry optimization process is carried out using an advanced algorithm that incorporates various optimization techniques, such as steepest descent, to minimize the energy of each structure. The convergence tolerances for energy and force are 0.0001 kcal/mol and 0.005 kcal/mol/Å, respectively, in accordance with the fine quality convergence criteria outlined in the Material Studio documentation To relax the structures at physiological

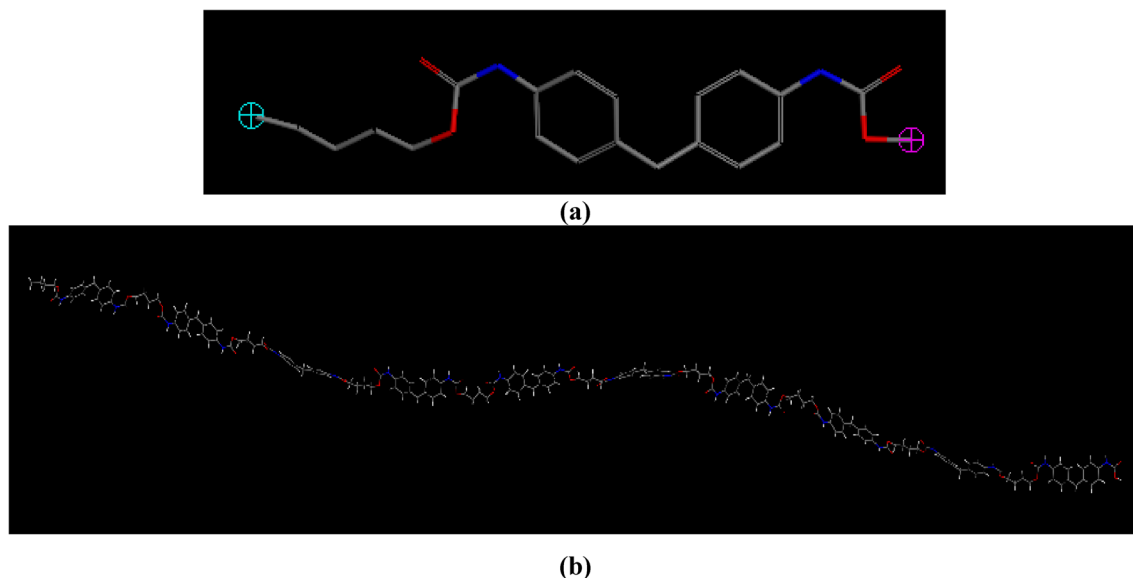


**Fig. 1.** Molecular structure of TPU (a) a monomer (b) an oligomer composed of 10 monomers.

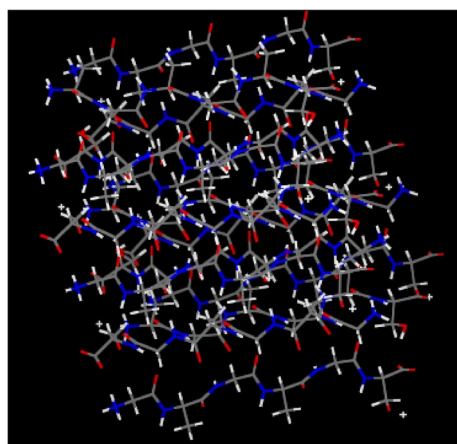


**Fig. 2.** Molecular structure of SF.

temperature, a dynamic simulation is performed for each structure using the NVT ensemble at 310 K for a duration of 300 ps, with a time step of 1 fs. The Berendsen thermostat is employed for temperature control during this phase.

In order to generate the model of scaffold surface, it is more computationally efficient to initially construct a small unit cell consisting of TPU and SF with a defined composition. This unit cell can then be replicated in both the x and y directions within Cartesian coordinates to generate the final scaffold surface.

To construct a cell of the above-mentioned polymers, the Amorphous Cell module within Material Studio software is utilized. Different amounts of TPU oligomers and SF molecules are incorporated into a cell with a density of 1.3 g/cm<sup>3</sup>, which closely matches the densities of both TPU and SF. The number of loaded molecules in each cell is affected by both their molecular weight and the composition of the scaffold. This study investigates three scaffolds with different compositions, and specific details for each scenario can be found in Table 1. After constructing the unit cell, the energy of each unit cell is minimized using a smart, high-quality algorithm. In the next step, each cell was subjected to annealing using the NVT ensemble, transitioning from an initial temperature of 300 K to a mid-cycle temperature of 450 K over a duration of 2 ns, with a time step of 1 fs. The total number of cycles is set at 1, with 5 heating ramps allocated for each cycle. The Berendsen thermostat is employed to control the temperature, and after each cycle, the structure is subjected to geometric optimization. The annealing step is crucial in the simulation process, as it helps prevent the system from becoming stuck in a local minimum, which could lead to unrealistic outcomes. Following the construction and relaxation of the polymeric unit cell, it is duplicated 3 times along the x and y axes to create the final scaffold model. The replication occurs in a plane that is perpendicular to the thickness of the cell. The energy of the generated supercell is minimized using a smart algorithm that ensures high quality. Subsequently, the optimized supercell

			One Unit Model			Bulk Models		
Composition	TPU (%)	SF (%)	$n_{TPU}$	$n_{SF}$	Dimension	$n_{TPU}$	$n_{SF}$	Dimension
SF:TPU-7/3	30	70	3	4	47.68Å*47.68Å*20Å	27	36	143.05Å*143.05Å*20Å
SF:TPU-1/1	50	50	4	4	47.98Å*47.98Å*20Å	36	36	143.94Å*143.94Å*20Å
SF:TPU-3/7	70	30	7	2	48.30Å*48.30Å*20Å	63	18	144.91Å*144.91Å*20Å
			Density(g/cc)		1.3	Density(g/cc)		1.3

**Table 1.** Properties used for construction of the unit cell and supercell of the polymeric surfaces.

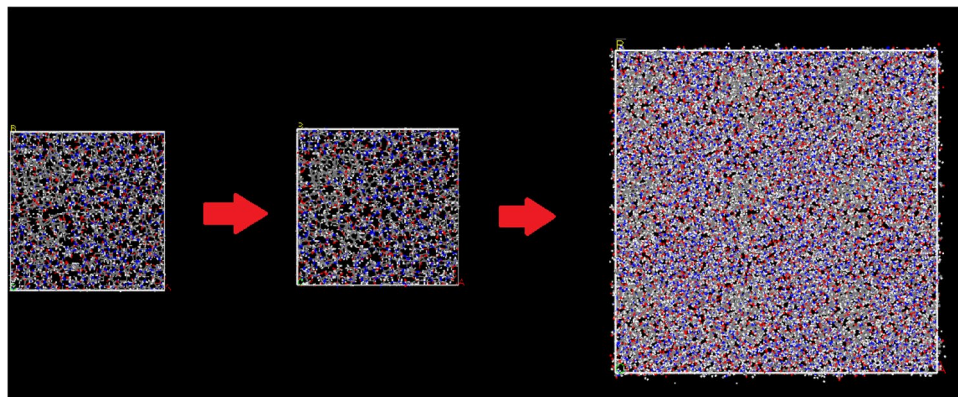


**Fig. 3.** In-cell representation of the unit and bulk models of the polymeric surfaces before and after performed simulations for equilibrium. (SF:TPU-7/3).

undergoes annealing using NVT ensemble for a duration of 3.5 ns, with other parameters configured similarly to those used in the unit cell annealing simulation, to achieve a homogeneous distribution of polymers within the supercell. Following this step, additional geometry optimization of the structure is performed. The annealed cells and supercells corresponding to the composition of SF:TPU-7/3 are represented in Fig. 3.

### Modeling protein structures

The structure of fibronectin (PDB ID: 1FBR) and laminin (PDB ID: 4YEQ) were obtained from the Protein Data Bank ([www.rcsb.org](http://www.rcsb.org)). Following several modifications using VMD 1.9.3 software, these structures were subsequently imported into Material Studio.

#### Fibronectin

Fibronectin is a glycoprotein found in the ECM that plays an important role in cell adhesion. Previous studies has identified 1FBR, which consists of 3 antiparallel  $\beta$ -sheets and contains 93 residues, as a candidate for investigating the cell adhesion characteristics of scaffolds<sup>30</sup>. The structure of this protein is depicted in Fig. 4.

#### Laminin

Laminin is the most abundant structural noncollagenous glycoproteins that can be found in the basement membrane that supports the endothelium. The N-terminal region of laminin features three polypeptide arms, designated as  $\alpha$ ,  $\beta$  and  $\gamma$ , are linked to the C-terminal through an extended  $\alpha$ -helical coiled coil structure. These shorter arms play a crucial role in interactions with cell surfaces, particularly in adhesion processes. The  $\alpha 2L4b$  domain is identified as the key component responsible for cell adhesion, and the protein 4YEQ, comprising 181 residues and exhibiting an antiparallel  $\beta$ -sandwich fold, is highlighted in this context (Fig. 5)<sup>31</sup>.

#### Relaxation of protein

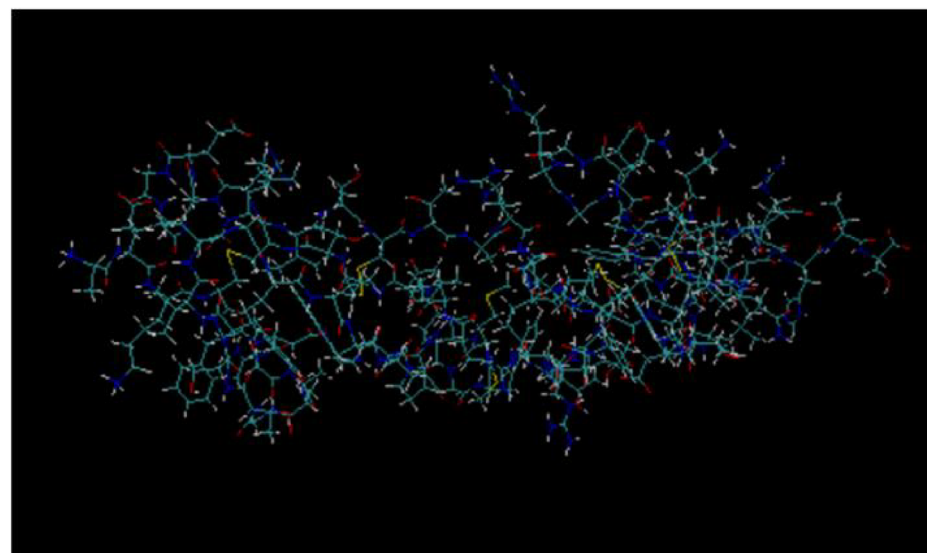
In order to simulate the behavior of proteins in live cell environments, the proteins were introduced into a water box following the addition of hydrogen atoms to the PDB files and subsequent optimization of their geometry. Energy minimization was performed utilizing the Smart algorithm, which incorporated a combination of steepest descent, conjugate gradient, quasi-Newton, and ABR methods, achieving a convergence tolerance of 0.001kcal/mol.

#### Layer construction

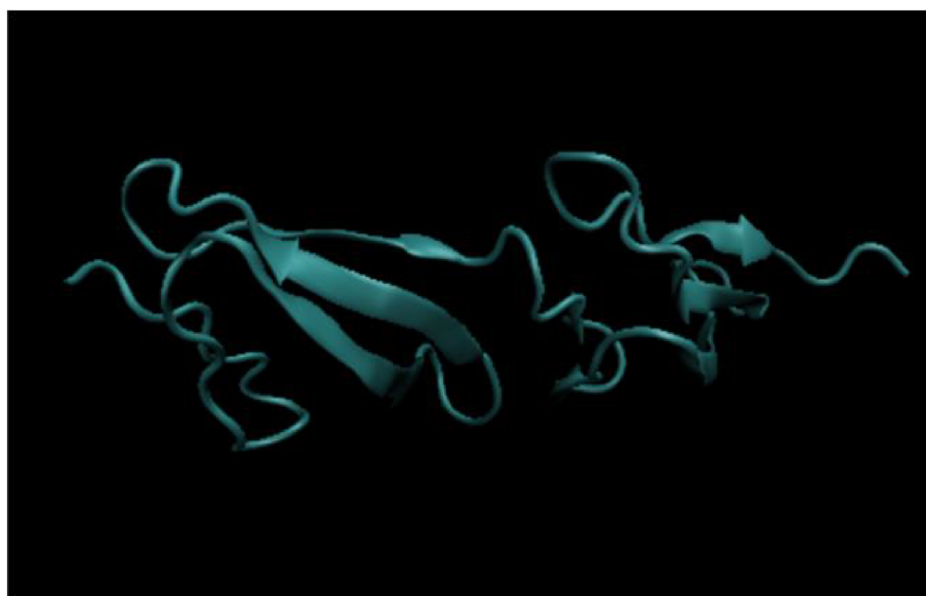
To assess the adhesion of proteins, the relaxed proteins were integrated into a layer situated above a polymeric scaffold featuring its annealed supercell. In order to minimize the influence of the upper wall of the layer, a vacuum of 300 Å was applied for the proteins, while a vacuum of 10 Å was utilized for the polymeric scaffold.

Simulation of protein-scaffold interaction.





(a)



(b)

**Fig. 4.** (a) Molecular structure of fibronectin, (b) secondary structure of fibronectin.

To study the interaction between the protein and the scaffold, the protein cell is positioned above a polymeric supercell. The protein cell is extended up to 300 Å in the direction of the polymeric surface thickness to prevent any unphysical interactions with the artificial layer above. Additionally, a gap of 10 Å is maintained between the polymeric surface and the protein cell. The energy of the resulting generated layered structure is minimized, followed by, a dynamic simulation conducted using the NVT ensemble at a temperature of 310 K for a duration of 500 ps, with a time step of 1 fs, employing the Berendsen method for temperature regulation. It is noteworthy that the atoms of the polymeric surface remain fixed during the simulations, while the protein atoms are allowed to move freely completely free. After performing the dynamic simulations, the adhesion energy can be calculated using the following expression<sup>1</sup>.

$$E_{adhesion} = (E_{protein} + E_{biomaterial}) - E_{total} \quad (7)$$

$E_{protein}$  and  $E_{biomaterial}$  represent the energy associated with the protein and polymeric surface prior to reaching equilibrium, while  $E_{total}$  denotes the energy of the system once equilibrium has been achieved. Given that the atoms of polymeric surface remain fixed throughout the simulations,  $E_{biomaterial}$  is assigned a value of zero. As indicated in Eq. (7), higher positive values of adhesion energy indicate a stronger adhesion of the

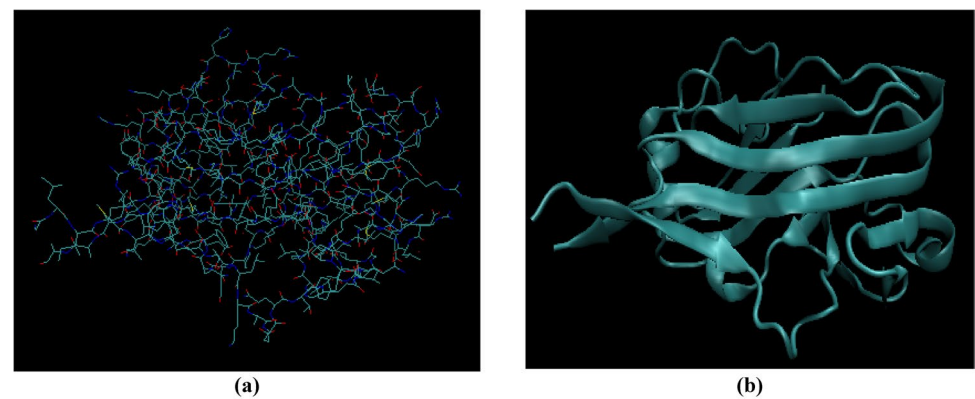


**Fig. 5.** (a) Molecular structure of laminin, (b) secondary structure of laminin.

Sample	Voltage (kV)		Flow rate (mL/h)		Distance (cm)		Temperature (°C)
	SF	TPU	SF	TPU	SF	TPU	
SF:TPU-7/3	15.7	18	1.2	0.5	24	16	25
SF:TPU-1/1	15.7	18	1	1	24	16	25
SF:TPU-3/7	15.7	18	0.3	0.8	24	16	25

**Table 2.** Parameters considered for electrospinning process.

protein to the scaffold surface, whereas lower values suggest a weaker adhesion. Moreover, negative values of adhesion energy may be considered as unsuccessful protein attachment to the polymeric surface.

Experimental

Co-electrospinning PU/SF

Tissue-engineered vascular grafts (TEVGs) are increasingly being created using electrospinning because of its capability to address key issues in treating cardiovascular disease. A potential benefit for electrospun TEVGs is that they can mimic the mechanical properties of native tissues, promote long-term patency, and facilitate tissue growth. By adjusting the process parameters, the geometrical, mechanical, and biological characteristics of nanofibers can be quickly controlled<sup>15,32</sup>. For fabricating the samples, PU was dissolved in a solution of Tetrahydrofuran (THF)/ Dimethylformamide (DMF) in a 3:1 ratio, while silk fibroin (SF) was produced in accordance with prior research<sup>33</sup>. Initially, 5 g of Bombyx Mori silk cocoons were cut into smaller pieces and boiled in a 0.02 M sodium carbonate solution for 30 min. The cocoons were then rinsed 3 times with distilled water for 20 min each and allowed to dry. The dry cocoons were immersed in a 9.3 M lithium bromide solution at a temperature of 60 °C for a duration of 4 h, followed by a 48-h dialysis in purified water. Upon completion of the dialysis, the resulting fibroin solution underwent centrifugation for 30 min to remove any impurities. Subsequently, a mixture of Polyethylene Oxides (PEO) and SF in a ratio of 1:3 was prepared<sup>15</sup>. Since the amount of the SF solution in the final mixture is three times that of the PEO solution and given that the mass concentration of the PEO solution (1.5%) is lower compared to the SF solution (8%), the mass fraction of PEO in the final sample is negligible. This allows the simulation results to be used as tool to predict the effect of the SF:TPU ratio on the protein absorption mechanism and strength.

The nanofibers were fabricated by loading the solutions into syringes equipped with 18 gauge blunt-ended needles positioned on both sides of a collector rotating at 900 rpm. The parameters including voltage, flow rate, distance from the collector, and temperature are detailed in the Table 2. The blending ratios of SF: TPU (30%, 50%, 70%) were determined based on the specific volumes of TPU and SF used during the electrospinning process.

Sample characterization

To investigate the morphology of the samples a scanning electron microscope (SEM) (Seron AIS2300C) was used. The hydrophilicity of the samples was evaluated using a drop shape analyzer, which involved measuring the contact angle of water droplets on the surfaces. The hydrophilic properties of the samples were quantified with a G10 goniometer (Jikan CAG-10 SE, Jikan Company), where an increased water contact angle denotes greater hydrophobicity, while a decreased water contact angle signifies enhanced hydrophilicity.

MTT cell viability assay.

To quantitatively measure the biocompatibility of the samples, cell viability and attachment were evaluated using the MTT assay. The study utilized third-passage human umbilical vein cells (HUVEC). Initially, the samples underwent sterilization by immersion in a 70% ethanol solution for 24 h, followed by exposure to UV rays

from all angles for one hour, and were subsequently rinsed with sterile Phosphate-Buffered saline (PBS). After sterilization, the samples were placed in Dulbecco's Modified of Eagle Medium (DMEM) supplemented with 10% fetal bovine serum (FBS) and incubated at 37 °C in a 5% CO<sub>2</sub> atmosphere for 24 h. Following this incubation period, the medium was removed, and cells at a density of  $5 \times 10^4 \frac{\text{cell}}{\text{well}}$  were seeded onto the samples. For the control group, an equivalent density of cells was seeded in an empty well. Finally, a fresh cell culture medium consisting of 89% DMEM, 10% FBS, and 1% penicillin/streptomycin was added to each well.

The MTT assay was conducted on days 1, 3, and 7 following the initial seeding on the the samples<sup>15,34,35</sup>. On these specified days, 500 µL of the culture medium was replaced with 50 µL of MTT solution, followed by a 3-h incubation period. Subsequently, the medium was replaced with 500 µL of dimethyl sulfoxide (DMSO) in order to facilitate the dissolution of the violet formazan in living cells. The cell proliferation for each sample was measured using an Elisa plate reader at 570 nm (Eq. 8). This test was repeated 3 times for each sample ( $n = 3$ ).

$$\text{Cellviability}\% = \frac{\text{Opticaldensityofthesample}}{\text{Opticaldensityofthecontrolgroup}} \times 100 \tag{8}$$

There is a direct relationship between the number of viable cells and the optical density measured in the MTT assays (a higher number of cells leads to a greater optical density), which enables precise measurement of cell proliferation rates<sup>23,24</sup>.

**Cell adhesion**

The cellular morphology was studied using a scanning electron microscope (SEM). In alignment with the previously described cell culture procedure, 40,000 HUVEC cells were inoculated onto each sample and incubated at 37 °C. On the 3<sup>rd</sup> and 7<sup>th</sup> days post-seeding, the cell culture medium was replaced with glutaraldehyde (2.5% v/v) for a duration of 4 h to immobilize the cells. The samples were rinsed with PBS 3 times. Following this, they were sequentially immersed in different concentrations of ethanol (50%, 60%, 70%, 80%, 90%, and 100%) for 15 min each to facilitate cell dehydrate. The samples were subsequently prepared for SEM imaging (Seron AIS2300C).

**Live/dead assay**

Similar to the MTT assay, HUVEC cells were cultured on the samples for the live/dead test. After 3 and 7 days of incubation, the samples were stained with acridine orange/pyridium iodide (AO/PI) and then analyzed under a microscope (TCM 400, Labomed).

**Degradation rate analysis**

The in vitro degradation rate assessment of the scaffolds was conducted by calculating the weight loss of scaffolds submerged in PBS solution ( $pH = 7$ ) for 7 days. The initial weight of the samples ( $W_i$ ) was measured, and then the samples were incubated in PBS solution at 37°C. At certain intervals, the samples were taken out, rinsed, and weighed ( $W$ ). The degradation rate of the electrospun scaffolds was calculated using Eq. 9:

$$\text{Degradationrate}(\%) = \frac{W_i - W}{W_i} \times 100 \tag{9}$$

**Statistical analysis**

A mean and standard deviation were calculated for each set of quantitative data and reported as mean ± standard deviation. The probability value (p-value) was calculated using one-way or two-way analysis of variance (ANOVA) and a significance level of 0.05 or less was considered in each analysis<sup>36</sup>.

**Results and discussion**

**Simulation results**

Based on molecular dynamic simulations, Table 3 presents the adhesion energy of fibronectin and laminin for the three scaffolds under consideration. Notably, the table indicates that the adhesion energy is significantly affected by the surface composition. As the mass fraction of SF increases to 0.5 within the scaffold, the adsorption of both laminin and fibronectin onto the surface is enhanced, regardless of protein type, which results in improved cell adhesion characteristics of the structure. This observation suggests that there exists an optimal ratio of SF in the composite material that enhances the biocompatibility of the hybrid scaffold. Moreover, a comparison of the adhesion energies of the different proteins reveals that laminin exhibits a stronger adhesion to the scaffold

Protein	Composition	$E_{total}$ (kcal/mol)	$E_{Protein}$ (kcal/mol)	$E_{adhesion}$ (kcal/mol)
Fibronectin	SF:TPU-7/3	147.315	268.922	121.607
	SF:TPU-1/1	142.363	268.922	126.559
	SF:TPU-3/7	236.033	268.922	32.889
Laminin	SF:TPU-7/3	520.682	659.671	138.989
	SF:TPU-1/1	463.073	659.671	196.598
	SF:TPU-3/7	680.789	659.671	-21.118

**Table 3.** Adhesion energy of different proteins at the end of simulation.



surface than fibronectin. Specifically, the adhesion energy of laminin adhesion to SF:TPU-3/7 sample is negative, indicating that this protein doesn't interact with the polymeric surface.

In addition to the energy of adhesion, the ultimate conformation of proteins plays a crucial role in the interaction between proteins and surfaces. To achieve a more detailed understanding of the adsorption mechanism, this study examines the final conformations of the proteins. Figures 6, 7, and 8 show the initial and final conformations of fibronectin alongside three scaffolds. Additionally, Figs. 9, 10, and 11 indicate the initial and final conformations of laminin in conjunction with three scaffolds. In instances where the adhesion energy is positive, the protein undergoes significant conformational changes and attaches to the polymeric surface. Additionally, as the adhesion energy rises, the quantity of interacting residues also increases.

The finding of the current computational study indicate that enhancing the SF fraction in the scaffold to a level of 0.5 leads to an increase in the protein adsorption strength of the surface, thereby significantly improvement in scaffold biocompatibility. Consequently, it is essential to strike a balance between the contents of SF and TPU to develop the most effective scaffold for tissue engineering purposes. To achieve this aim, a range of compositions should be examined through computational methods, followed by validation of the results using MTT cell viability assays to identify the optimal composition.

## Experimental results

### Sample characterization

The samples with varying ratios were produced through the process of electrospinning, with the nanofiber morphology illustrated in Fig. 12(a–c). It is evident that the resulting fibers were free of any beads. The average diameter of SF:TPU-1/1, SF:TPU-3/7, and SF:TPU-7/3 were approximately  $(1.052 \pm 0.297) \mu\text{m}$ ,  $(1.353 \pm 0.624) \mu\text{m}$ , and  $(0.389 \pm 0.107) \mu\text{m}$ , respectively, which aligns with findings from earlier studies<sup>15,37</sup>.

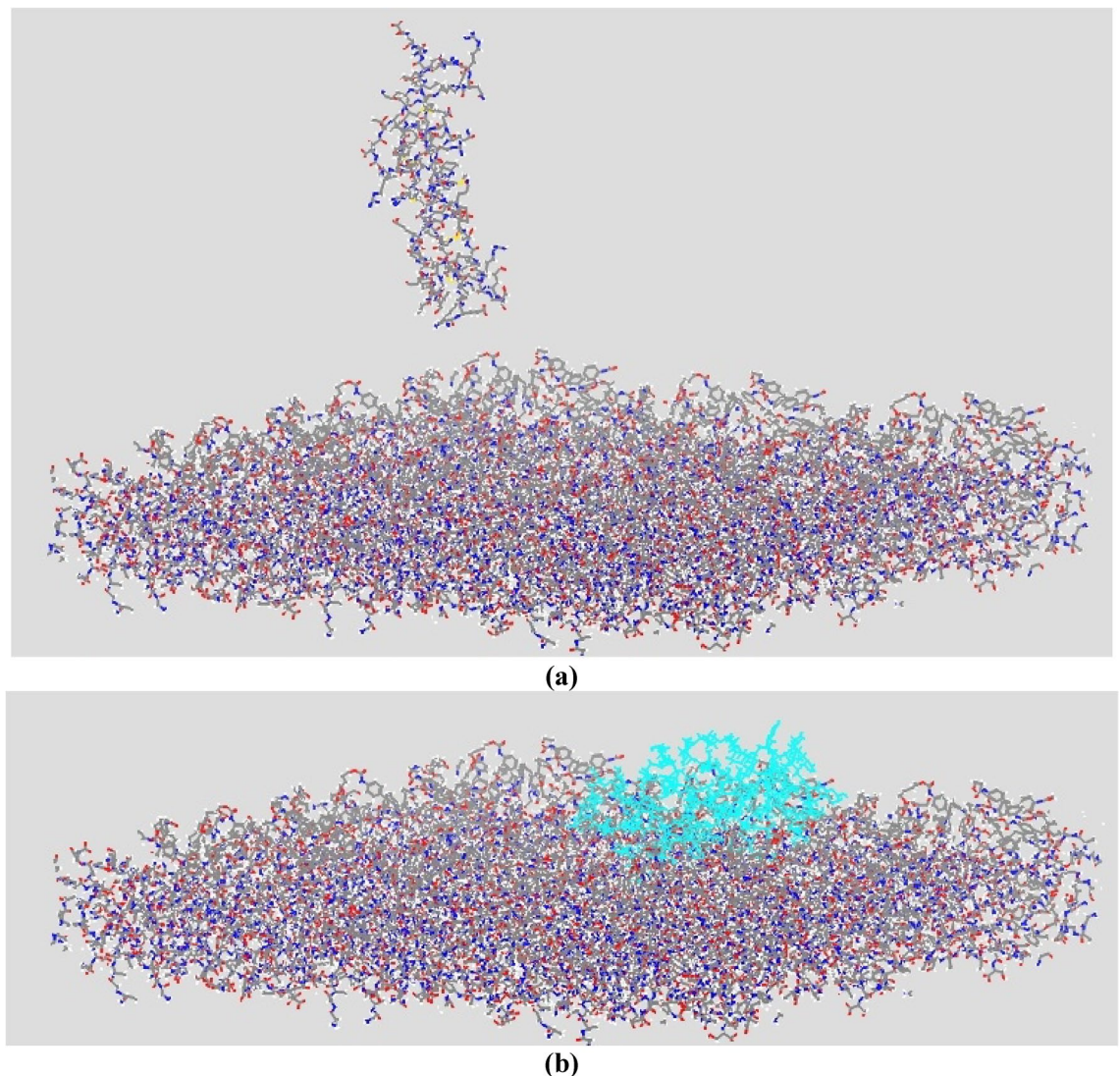


**Fig. 6.** (a)Initial, (b) Final configuration of layer (SF:TPU-7/3) with fibronectin.

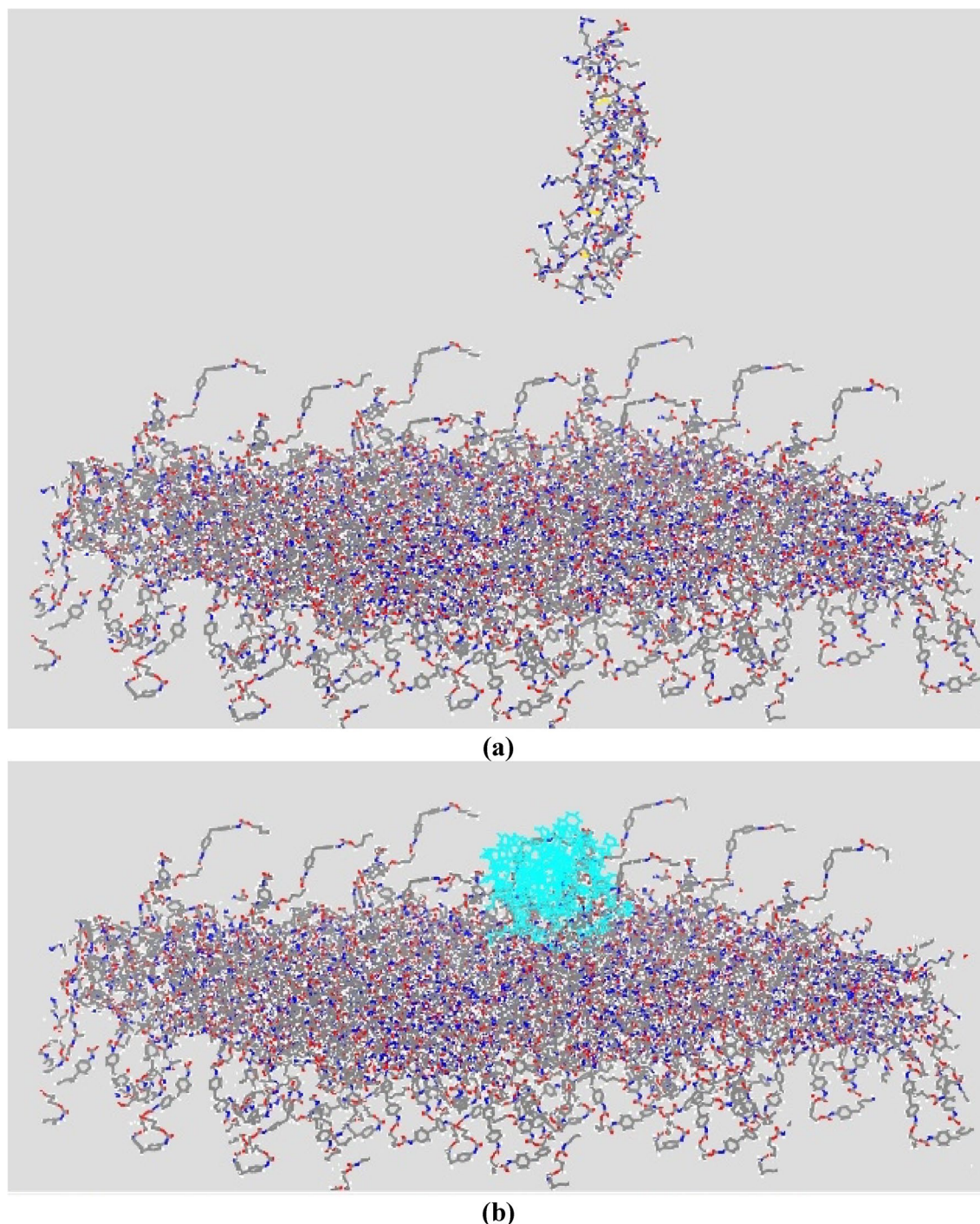


**Fig. 7.** (a)Initial, (b) Final configuration of layer (SF:TPU-1/1) with fibronectin.

The water contact angle for the samples is reported in Fig. 12(d). The analysis demonstrated that a reduction in TPU concentration led to an increase in the hydrophilicity of the substrate, suggesting that the hydrophilicity of the system influenced by the characteristics of the substrate. The SF:TPU-7/3 sample exhibited the greatest hydrophilicity due to its lower fibroin concentration, whereas the SF:TPU-3/7 sample displayed the least hydrophilicity<sup>38,39</sup>.

#### *MTT assay*

The MTT assay was performed using endothelial cells to quantitatively assess the viability of samples<sup>40</sup>. The results of the MTT assay for days 1, 3, and 7 of cell culture are illustrated in Fig. 12(e). In this research we utilized TCP (Tissue Culture Plate) acts as a reference standard, allowing for the comparison of the impacts of various substances on cell viability and metabolic activity. This ensures the proper functioning of the assay by providing



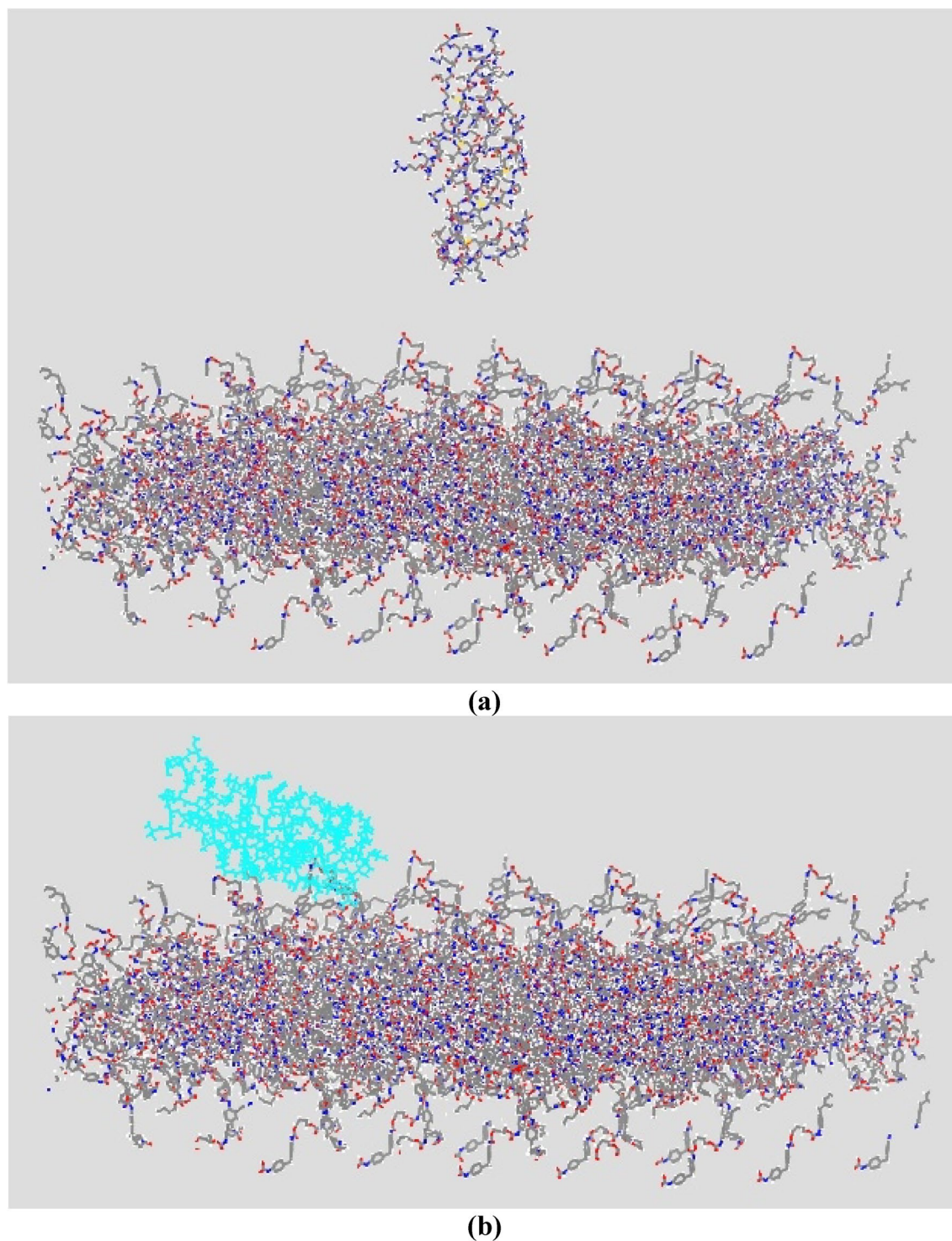


**Fig. 8.** (a)Initial, (b) Final configuration of layer (SF:TPU-3/7) with fibronectin.

a reliable benchmark for evaluating other experimental outcomes. The findings indicate that the ratios of the polymers affect the biocompatibility of the scaffolds. Notably, the SF:TPU-1/1 sample exhibited the highest cell viability. Furthermore, the optical density of the samples showed an increase from day 1 to day 7, suggesting the absence of cytotoxic effects in the fabricated samples. These results imply that a 50% SF content in the sample provides optimal biocompatibility, particularly for tissue engineering applications, as higher percentages of SF don't significantly enhance cell activity on the scaffolds. In general, samples with elevated SF content demonstrated greater biocompatibility. These findings are consistent with previously published studies<sup>15,41</sup>.

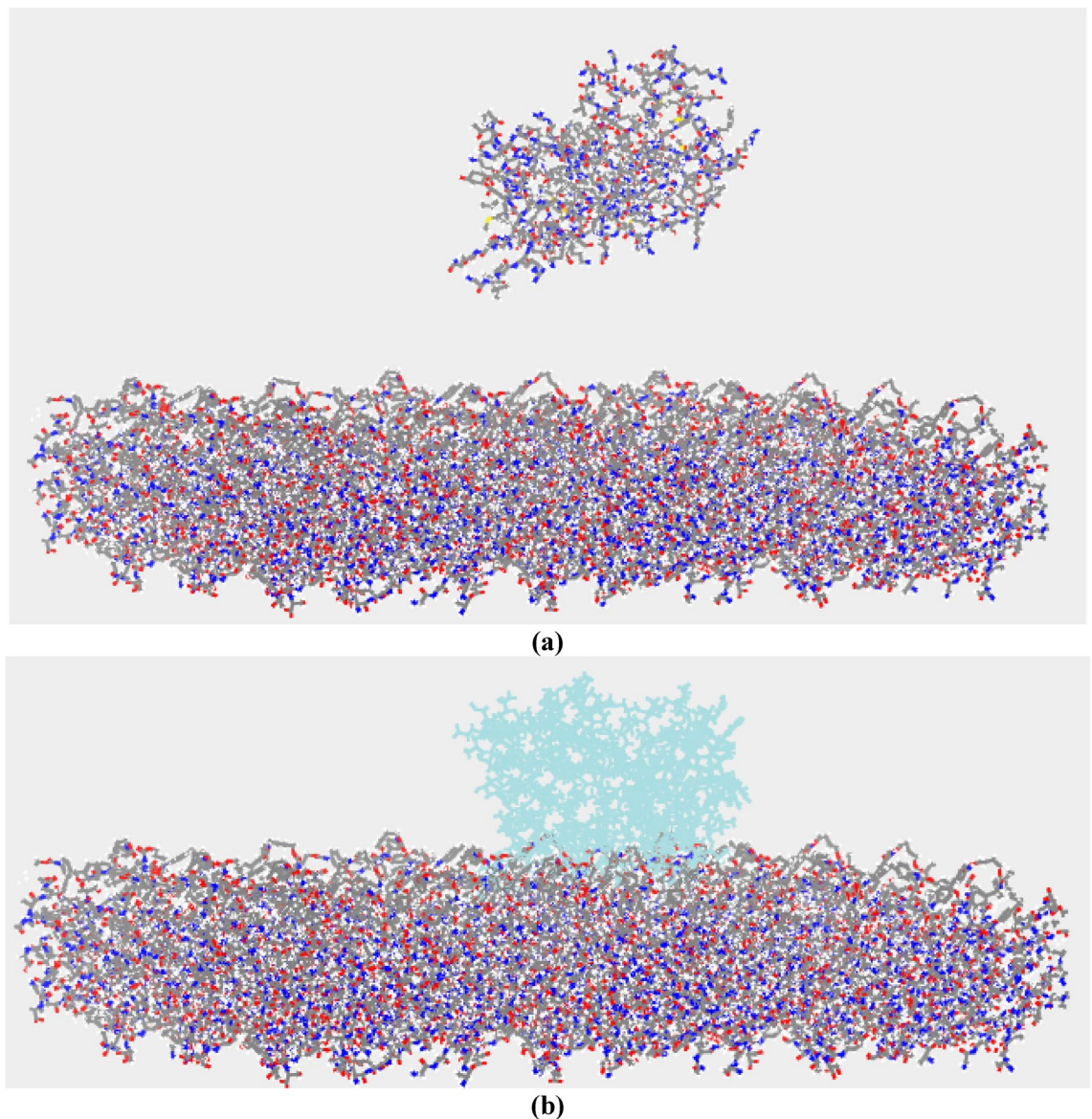


**Fig. 9.** (a)Initial, (b) Final configuration of layer (SF:TPU-7/3) with laminin.

#### *Cell adhesion*

The results of cell adhesion (Fig. 13) demonstrate a strong integration between the cells and the scaffold, as well as the initiation of an endothelial cell monolayer on the surface of the scaffolds, which is crucial for the successful implementation of the vascular graft. Furthermore, the SF: TPU-1/1 sample showed a more extensive endothelial cell layer and superior adhesion throughout the duration of the test, aligning with the findings from the MTT assay and simulation results. Notably, none of the adhered cells displayed a globular morphology, which suggests effective initial attachment and biocompatibility of the electrospun fibers<sup>42</sup>.

#### *Live/dead assay*

The results of the immunofluorescence staining for live/dead cells are shown in Fig. 14, which examines the morphology and growth factor of the cultured cells on days 3 and 7. It is evident that there was an increase in cell density from day 3 to day 7. Furthermore, the majority of the cells exhibited a bright green coloration, demonstrating that they successfully attached and proliferated on the fibers<sup>37</sup>. Notably, the cell count in the SF:TPU-3/7 sample was lower compared to the other two samples, which aligns with the findings from the MTT assay<sup>43,44</sup>.

#### *Degradation rate profile*

Assessment of the degradation rate of the scaffolds is crucial for effective tissue regeneration, as it ensures that the scaffolds degrade at a rate which allows proper cell infiltration and new tissue formation<sup>45</sup>. Figure 15 depicts SF:TPU electrospun scaffolds degradation results in PBS solution within 7 days at 37°C. The highest increase



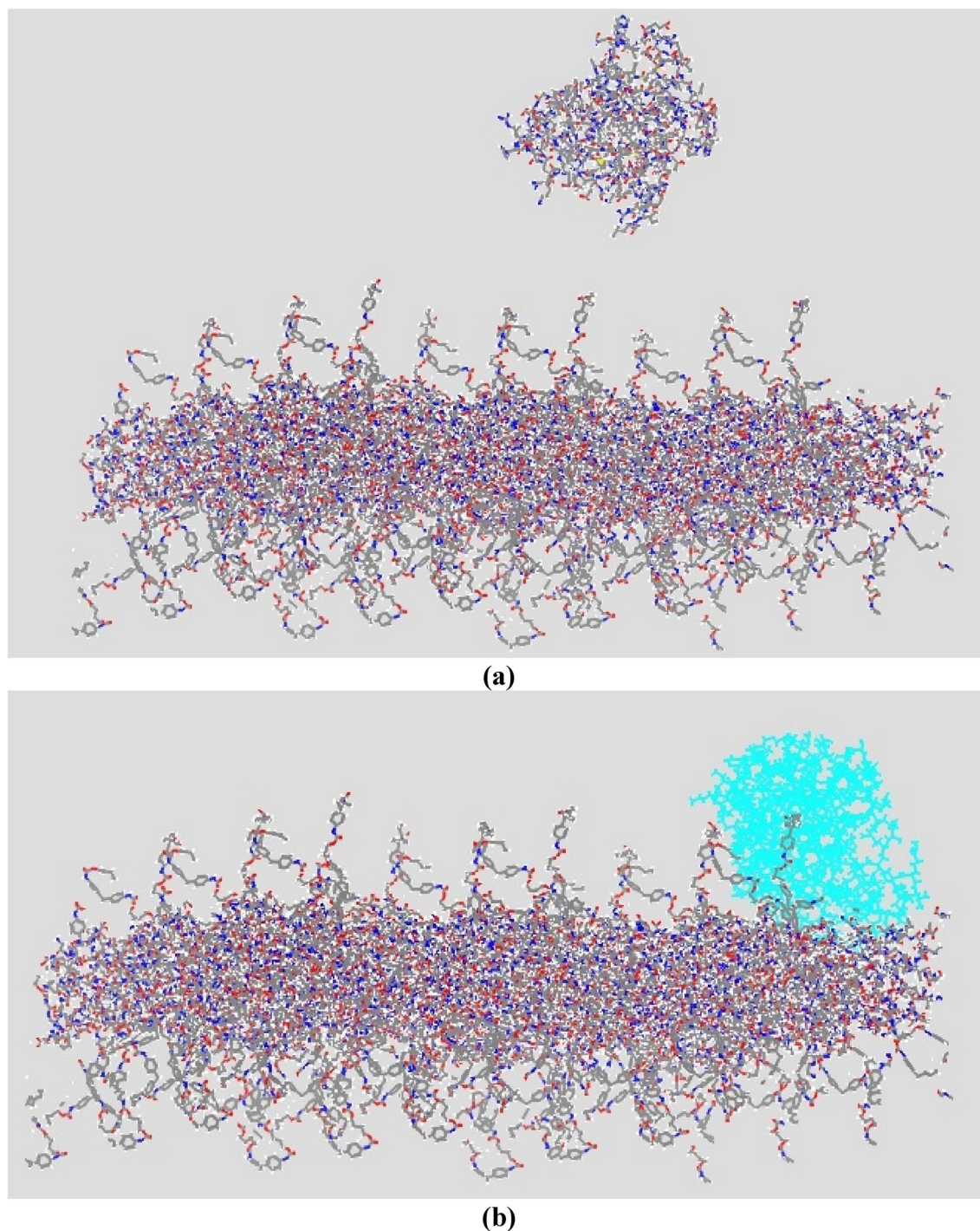


**Fig. 10.** (a)Initial, (b) Final configuration of layer (SF:TPU-1/1) with laminin.

in degradation rate occurred in the first 24 h, and thereafter, the degradation rate decreased for all the samples. Among the introduced groups, the SF:TPU-7/3 exhibited a higher degradation rate of 22.22, compared to the other groups. This can be attributed to the higher proportion of SF in the electrospun scaffold, which, due to the presence of hydrophilic functional groups such as hydroxyl groups in SF that facilitate water absorption, leads to a higher degradation rate compared to the TPU<sup>46</sup>. On the other hand, the TPU has a lower degradation rate compared to the SF, which is due to its higher chemical stability, stemming from amorphous and semi-crystalline structure that resists hydrolytic degradation more effectively than the SF  $\beta$ -sheet crystalline<sup>41</sup>. The degradation rate of the electrospun scaffold increases from  $2.127 \pm 0.457$ ,  $10.073 \pm 0.998$ ,  $12.886 \pm 1.006$  on day 1 to  $9.660 \pm 0.775$ ,  $15.648 \pm 1.231$ ,  $20.413 \pm 0.406$  on day 7, for SF:TPU-7/3, SF:TPU-5/5, and SF:TPU-3/7, respectively. By comparing these groups, the degradation rate of the scaffold decreased with the lowering content of SF in the electrospinning process relative to the TPU and the hydrophilicity of the scaffold.



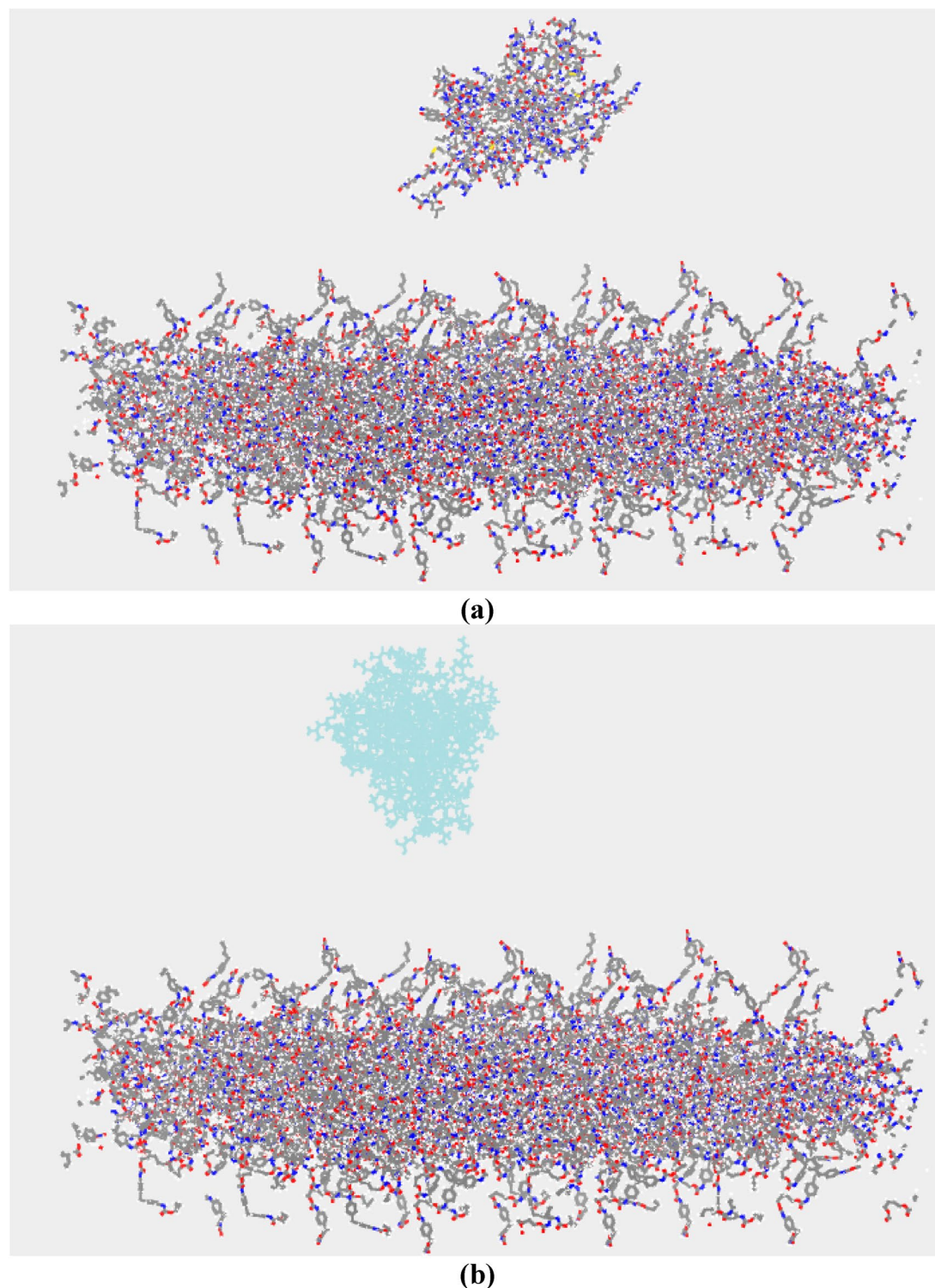


**Fig. 11.** (a)Initial, (b) Final configuration of layer (SF:TPU-3/7) with laminin.

## Discussion

In the experimental section, SF: TPU-1/1 exhibited the highest level of biocompatibility with HUVECS, as confirmed by cell proliferation obtained from the MTT assay, which were further substantiated through cell morphology studies. Simulations and experiments indicate that samples with higher SF contents do not promote cell adhesion or proliferation. This finding is consistent with the results of other studies<sup>36,41</sup>. There could be differences in the results of other assays due to the different experimental conditions and, most importantly, the different types of cells utilized during experiments<sup>36</sup>. The Live/Dead staining indicated that all the samples

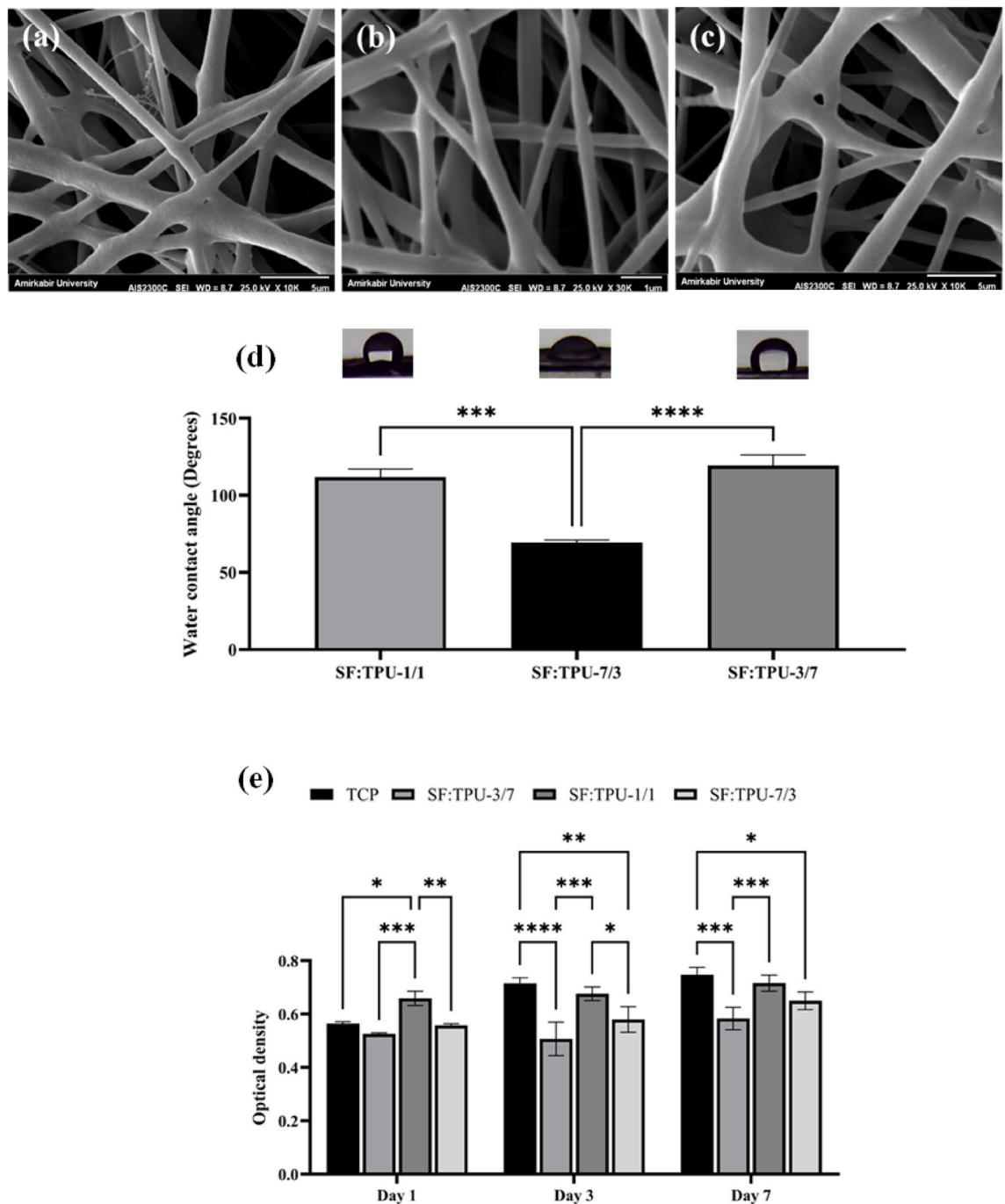


**Fig. 12.** SEMs for evaluation of Nanofiber morphology of (a) SF:TPU-1/1, (b) SF:TPU-7/3, (c) SF:TPU-3/7, (d) The hydrophilicity of the samples was assessed by measuring their water contact angle using a G10 goniometer (Jikan CAG-10 SE, Jikan Company) for quantification, (e) MTT assay results of days 1, 3, and 7 of cell culture. (\* indicates probability value  $p < 0.05$ , \*\* indicates  $p < 0.01$ , \*\*\* indicates  $p < 0.001$  and \*\*\*\* indicates  $p < 0.0001$ , the p-value was calculated using one-way (d) and two-way (e) ANOVA).

maintained excellent cell viability, predominantly featuring elongated green live cells adhering to the graft surface. Scanning SEM images revealed a flattened morphology of the attached cells across all the samples, indicative of healthy cellular activity and proliferation on the surface<sup>41</sup>. This phenomenon can be linked to the biostability of TPU combined with the presence of the RGD sequence in the structure of SF, which significantly improves cell adhesion<sup>47–49</sup>. Furthermore, an increase in TPU content led to the formation of more hydrophobic scaffolds with a larger average diameter.

A comparison of the contact angles of three samples revealed that SF:TPU-1/1, the most biocompatible, has a moderate contact angle compared with two other samples. Hydrophilicity is generally more favorable for cell adhesion; however, excessive SF content in SF:TPU-7/3 might have altered the conformation of proteins like

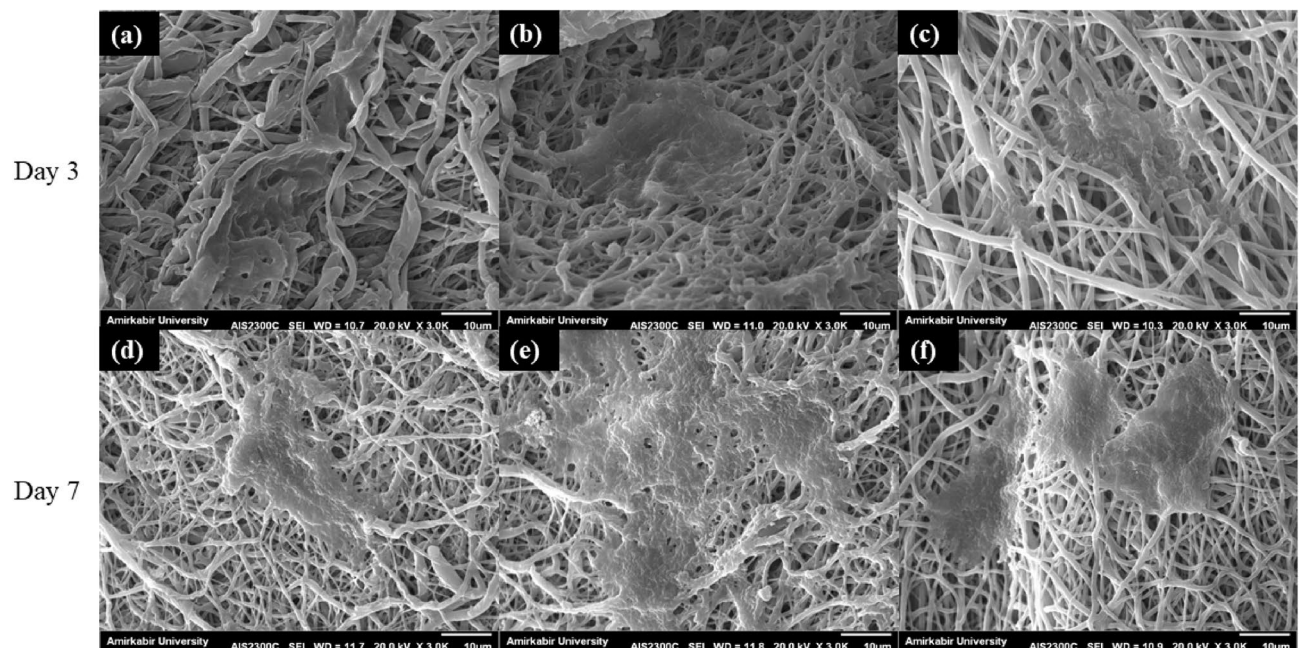


**Fig. 13.** 40,000 HUVEC cells were incubated at 37 °C, then treated with 2.5% glutaraldehyde for 4 h. The samples were washed three times with PBS and dehydrated using a 50% to 100% ethanol gradient for 15 min and SEM images of HUVEC cell morphology attached on the scaffold for the cell adhesion assay. (a, d) SF: TPU-3/7. (b, e) SF: TPU-1/1. (c, f) SF: TPU-7/3.

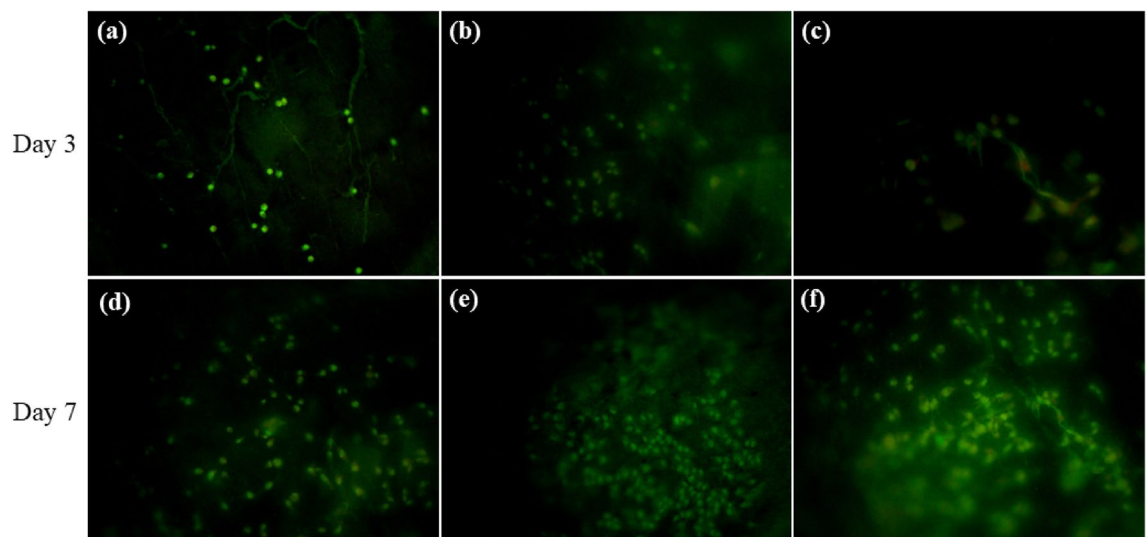


**Fig. 14.** HUVEC cells cultured on the samples were subjected to staining with acridine orange/pyridium iodide (AO/PI) after 3 and 7 days and subsequently examined using a Labomed TCM 400 microscope. Fluorescence images of HUVEC cells on the scaffold for the live/dead assay. (a, d) SF: TPU-3/7. (b, e) SF: TPU-1/1. (c, f) SF: TPU-7/3.

fibronectin and laminin, reducing their functional interactions with cells<sup>50</sup>. A similar result has been found in previous studies, which claim that extremely hydrophobic or hydrophilic surfaces exhibit poor cell adhesion due to weak protein adsorption. Meanwhile, moderately wettable surfaces show maximum cell adhesion and biocompatibility due to optimum absorption of ECM proteins, suggesting that the balance of hydrophilic and hydrophobic interactions in a composite scaffold better supports cellular activity<sup>50–52</sup>.



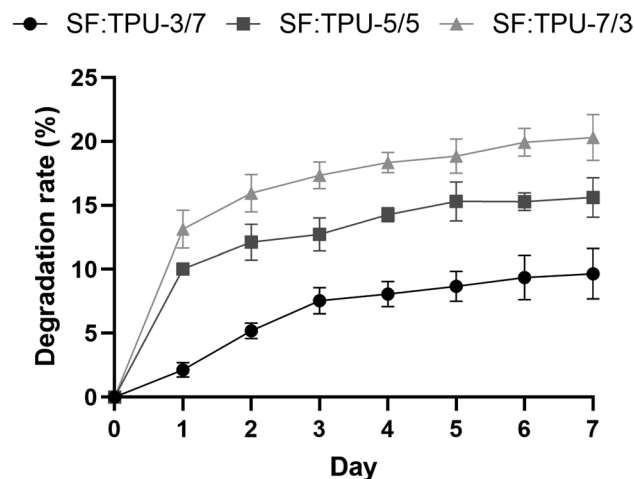


**Fig. 15.** Degradation rate profile of scaffolds in PBS within 7 days at 37 °C.

## Conclusion

In our previous studies, we developed numerical and experimental platforms for studying biological tissues<sup>1,7,12,15,16,30,35,53,54</sup>. This research employed Molecular Dynamics simulations in conjunction with experimental assays to investigate how composition influences the biocompatibility of a hybrid TPU-SF fibroin scaffold. The study focused on the relationship between cell adhesion and proliferation characteristics of biomaterials and their specific protein adsorption capabilities. Three distinct blends with varying compositions were analyzed: One containing 70% TPU, another with 50% TPU, and the last one comprising 30% TPU. In order to evaluate the cell adhesion potential of the polymeric surfaces, the adsorption of two key endothelial ECM proteins, fibronectin and laminin, was examined, taking into account adhesion energy and the final confirmation of the proteins. The simulation results indicated that increasing the SF content to 50% in the blend enhances adhesion energy, thereby improving the scaffold's to adsorb proteins, regardless of the protein type. Notably, laminin exhibited a stronger adhesion to the scaffold surface compared to fibronectin. The analysis of the final protein conformation showed that when the adhesion energy is negative, the protein does not contact the scaffold surface. Conversely, proteins with positive adhesion energy experienced significant conformational changes and adhered to the polymeric surface. The number of interacting residues was found to increase with higher adhesion energy. Experimental results corroborated the simulation results, demonstrating that biocompatibility can be effectively predicted through molecular dynamics simulations. Consequently, for tissue engineering applications, it is essential to achieve an optimal balance of SF and TPU contents. To find the ideal composition, further molecular dynamic simulations should be conducted to examine the biocompatibility of various blends.

## Data availability

The data that support the findings of this study are available from corresponding author on reasonable request.

Received: 11 October 2024; Accepted: 7 May 2025

Published online: 12 May 2025

## References

- Sarmadi, M., Shamloo, A. & Mohseni, M. Utilization of molecular dynamics simulation coupled with experimental assays to optimize biocompatibility of an electrospun PCL/PVA scaffold. *PLoS ONE* **12**(1), e0169451 (2017).
- Ghasemi-Mobarakeh, L., Prabhakaran, M. P., Morshed, M., Nasr-Esfahani, M.-H. & Ramakrishna, S. Electrospun poly( $\epsilon$ -caprolactone)/gelatin nanofibrous scaffolds for nerve tissue engineering. *Biomaterials* **29**(34), 4532–4539. <https://doi.org/10.1016/j.biomaterials.2008.08.007> (2008).
- Oh, S. H., Kang, S. G., Kim, E. S., Cho, S. H. & Lee, J. H. Fabrication and characterization of hydrophilic poly(lactic-co-glycolic acid)/poly(vinyl alcohol) blend cell scaffolds by melt-molding particulate-leaching method. *Biomaterials* **24**(22), 4011–4021. [https://doi.org/10.1016/s0142-9612\(03\)00284-9](https://doi.org/10.1016/s0142-9612(03)00284-9) (2003).
- Andrade, J. D. & Hlady, V. Protein adsorption and materials biocompatibility: a tutorial review and suggested hypotheses". *Biopolym. HPLC* [https://doi.org/10.1007/3-540-16422-7\\_6](https://doi.org/10.1007/3-540-16422-7_6) (1986).
- Rabe, M., Verdes, D. & Seeger, S. Understanding protein adsorption phenomena at solid surfaces. *Adv. Colloid Interface Sci.* **162**(1–2), 87–106 (2011).
- Raffaini, G. & Ganazzoli, F. Simulation study of the interaction of some albumin subdomains with a flat graphite surface. *Langmuir* **19**(8), 3403–3412 (2003).
- Heidari, H. & Shamloo, A. The effect of rippled graphene sheet roughness on the adhesive characteristics of a collagen–graphene system. *Int. J. Adhes. Adhes.* **64**, 9–14 (2016).
- Regis, S. et al. Fibronectin adsorption on functionalized electrospun polycaprolactone scaffolds: Experimental and molecular dynamics studies. *J. Biomed. Mater. Res. Part A* **102**(6), 1697–1706 (2014).
- Ebrahimi, S., Ghafoori-Tabrizi, K. & Rafii-Tabar, H. Molecular dynamics simulation of the adhesive behavior of collagen on smooth and randomly rough TiO<sub>2</sub> and Al<sub>2</sub>O<sub>3</sub> surfaces. *Comput. Mater. Sci.* **71**, 172–178 (2013).

10. Raffaini, G. & Ganazzoli, F. Understanding the performance of biomaterials through molecular modeling: crossing the bridge between their intrinsic properties and the surface adsorption of proteins. *Macromol. Biosci.* **7**(5), 552–566 (2007).
11. H. Shaygani *et al.*, Novel bilayer coating on gentamicin-loaded titanium nanotube for orthopedic implants applications, *Int. J. Pharm.*, 122764, (2023).
12. Seifi, S., Bakhtiari, M. A., Shaygani, H., Shamloo, A. & Almasi-Jaf, A. Investigating the correlation between the protein adhesion simulation and the biocompatibility of polymeric substrate for skin tissue engineering applications. *Phys. Chem. Chem. Phys.* <https://doi.org/10.1039/D2CP05763H> (2023).
13. Tatai, L. *et al.* Thermoplastic biodegradable polyurethanes: The effect of chain extender structure on properties and in-vitro degradation. *Biomaterials* **28**(36), 5407–5417. <https://doi.org/10.1016/j.biomaterials.2007.08.035> (2007).
14. Ajili, S. H., Ebrahimi, N. G. & Khorasani, M. T. Study on thermoplastic polyurethane/polypropylene (TPU/PP) blend as a blood bag material. *J. Appl. Polym. Sci.* **89**(9), 2496–2501 (2003).
15. Maleki, S., Shamloo, A. & Kalantarnia, F. Tubular TPU/SF nanofibers covered with chitosan-based hydrogels as small-diameter vascular grafts with enhanced mechanical properties. *Sci. Rep.* **12**(1), 1–15 (2022).
16. Almasi-Jaf, A., Shamloo, A., Shaygani, H. & Seifi, S. Fabrication of heparinized bi-layered vascular graft with PCL/PU/gelatin co-electrospun and chitosan/silk fibroin/gelatin freeze-dried hydrogel for improved endothelialization and enhanced mechanical properties. *Int. J. Biol. Macromol.* <https://doi.org/10.1016/j.ijbiomac.2023.126807> (2023).
17. Tungtasana, H. *et al.* Tissue response and biodegradation of composite scaffolds prepared from Thai silk fibroin, gelatin and hydroxyapatite. *J. Mater. Sci. Mater. Med.* **21**(12), 3151–3162. <https://doi.org/10.1007/s10856-010-4159-5> (2010).
18. Zhang, X., Baughman, C. B. & Kaplan, D. L. In vitro evaluation of electrospun silk fibroin scaffolds for vascular cell growth. *Biomaterials* **29**(14), 2217–2227. <https://doi.org/10.1016/j.biomaterials.2008.01.022> (2008).
19. Srisuwan, Y., Srihanam, P. & Baimark, Y. Preparation of silk fibroin microspheres and its application to protein adsorption. *J. Macromol. Sci. Part A Pure Appl. Chem.* **46**, 521–525 (2009).
20. Farokhi, M. *et al.* Silk fibroin scaffolds for common cartilage injuries: Possibilities for future clinical applications. *Eur. Polym. J.* **115**, 251–267. <https://doi.org/10.1016/j.eurpolymj.2019.03.035> (2019).
21. Sadeghi, A., Moztaazadeh, F. & Aghazadeh Mohandesi, J. Investigating the effect of chitosan on hydrophilicity and bioactivity of conductive electrospun composite scaffold for neural tissue engineering. *Int. J. Biol. Macromol.* <https://doi.org/10.1016/j.ijbiomac.2018.10.022> (2019).
22. Thottappillil, N. & Nair, P. D. Scaffolds in vascular regeneration: current status. *Vasc. Health Risk Manag.* **11**, 79 (2015).
23. Zund, G. *et al.* Tissue engineering in cardiovascular surgery: MTT, a rapid and reliable quantitative method to assess the optimal human cell seeding on polymeric meshes. *Eur. J. Cardio-thoracic Surg.* **15**(4), 519–524 (1999).
24. M. Ghasemi, T. Turnbull, S. Sebastian, and I. Kempson, The MTT Assay: Utility, Limitations, Pitfalls, and Interpretation in Bulk and Single-Cell Analysis., *Int. J. Mol. Sci.*, <https://doi.org/10.3390/ijms22312827>. (2021).
25. Mayo, S. L., Olafson, B. D. & Goddard, W. A. DREIDING: a generic force field for molecular simulations. *J. Phys. Chem.* **94**(26), 8897–8909 (1990).
26. Talapatra, A. & Datta, D. Estimation of improvement in elastic moduli for functionalised defective graphene-based thermoplastic polyurethane nanocomposites: a molecular dynamics approach. *Mol. Simul.* **47**(7), 602–618 (2021).
27. Zhong, J. *et al.* Self-assembly of regenerated silk fibroin from random coil nanostructures to antiparallel  $\beta$ -sheet nanostructures. *Biopolymers* **101**(12), 1181–1192 (2014).
28. Grant, A. M. *et al.* Silk fibroin–substrate interactions at heterogeneous nanocomposite interfaces. *Adv. Funct. Mater.* **26**(35), 6380–6392 (2016).
29. Patel, M., Dubey, D. K. & Singh, S. P. Phenomenological models of Bombyx mori silk fibroin and their mechanical behavior using molecular dynamics simulations. *Mater. Sci. Eng. C* **108**, 110414 (2020).
30. Shamloo, A. & Sarmadi, M. Investigation of the adhesive characteristics of polymer–protein systems through molecular dynamics simulation and their relation to cell adhesion and proliferation. *Integr. Biol.* **8**(12), 1276–1295 (2016).
31. Moran, T., Gat, Y. & Fass, D. Laminin L4 domain structure resembles adhesion modules in ephrin receptor and other transmembrane glycoproteins. *FEBS J.* **282**(14), 2746–2757 (2015).
32. Rickel, A. P., Deng, X., Engebretson, D. & Hong, Z. Electrospun nanofiber scaffold for vascular tissue engineering. *Mater. Sci. Eng. C. Mater. Biol. Appl.* <https://doi.org/10.1016/j.msec.2021.112373> (2021).
33. Rockwood, D. N. *et al.* Materials fabrication from Bombyx mori silk fibroin. *Nat. Protoc.* **6**(10), 1612–1631 (2011).
34. Zhao, X. *et al.* A novel injectable sodium alginate/chitosan/sulfated bacterial cellulose hydrogel as biohybrid artificial pancreas for real-time glycaemic regulation. *Carbohydr. Polym.* <https://doi.org/10.1016/j.carbpol.2025.123323> (2025).
35. Shaygani, H., Shamloo, A., Akbarataj, K. & Maleki, S. In vitro and in vivo investigation of chitosan/silk fibroin injectable interpenetrating network hydrogel with microspheres for cartilage regeneration. *Int. J. Biol. Macromol.* <https://doi.org/10.1016/j.ijbiomac.2024.132126> (2024).
36. Park, H. *et al.* Silk fibroin–polyurethane blends: Physical properties and effect of silk fibroin content on viscoelasticity, biocompatibility and myoblast differentiation. *Acta Biomater.* **9**(11), 8962–8971 (2013).
37. Mi, H.-Y. *et al.* Manipulating the structure and mechanical properties of thermoplastic polyurethane/polycaprolactone hybrid small diameter vascular scaffolds fabricated via electrospinning using an assembled rotating collector. *J. Mech. Behav. Biomed. Mater.* **78**, 433–441 (2018).
38. Mi, H.-Y. *et al.* Fabrication of triple-layered vascular grafts composed of silk fibers, polyacrylamide hydrogel, and polyurethane nanofibers with biomimetic mechanical properties. *Mater. Sci. Eng. C* **98**, 241–249 (2019).
39. Bazgir, M. *et al.* Fabrication and characterization of PCL/PLGA coaxial and bilayer fibrous scaffolds for tissue engineering. *Materials (Basel)* **14**(21), 6295 (2021).
40. Zavan, B. *et al.* Electrospun PCL-based vascular grafts: In vitro tests. *Nanomaterials* **11**(3), 751 (2021).
41. Yu, E., Mi, H., Zhang, J., Thomson, J. A. & Turng, L. Development of biomimetic thermoplastic polyurethane/fibroin small-diameter vascular grafts via a novel electrospinning approach. *J. Biomed. Mater. Res. Part A* **106**(4), 985–996 (2018).
42. Mi, H. *et al.* Fabrication and modification of wavy multicomponent vascular grafts with biomimetic mechanical properties, antithrombogenicity, and enhanced endothelial cell affinity. *J. Biomed. Mater. Res. Part B Appl. Biomater.* **107**, 2397–2408 (2019).
43. Vishwanath, V., Pramanik, K. & Biswas, A. Optimization and evaluation of silk fibroin–chitosan freeze-dried porous scaffolds for cartilage tissue engineering application. *J. Biomater. Sci. Polym. Ed.* **27**(7), 657–674 (2016).
44. Do, T. M., Yang, Y. & Deng, A. Porous bilayer vascular grafts fabricated from electrospinning of the recombinant human collagen (RHC) peptide-based blend. *Polymers (Basel)* **13**(22), 4042 (2021).
45. Alasvand, N. *et al.* Tissue-engineered small-diameter vascular grafts containing novel copper-doped bioactive glass biomaterials to promote angiogenic activity and endothelial regeneration. *Mater. Today Bio* <https://doi.org/10.1016/j.mtbio.2023.100647> (2023).
46. Xu, D. *et al.* Degradation profiles of the poly( $\epsilon$ -caprolactone)/silk fibroin electrospinning membranes and their potential applications in tissue engineering. *Int. J. Biol. Macromol.* <https://doi.org/10.1016/j.ijbiomac.2024.131124> (2024).
47. Shimada, R. *et al.* Development of a new surgical sheet containing both silk fibroin and thermoplastic polyurethane for cardiovascular surgery. *Surg. Today* **48**, 486–494 (2018).
48. Lee, J.-K., Lim, H.-S. & Kim, J.-H. Cytotoxic activity of aminoderivatized cationic chitosan derivatives. *Bioorg. Med. Chem. Lett.* **12**(20), 2949–2951 (2002).
49. Pankongadisak, P. & Suwantong, O. Enhanced properties of injectable chitosan-based thermogelling hydrogels by silk fibroin and longan seed extract for bone tissue engineering. *Int. J. Biol. Macromol.* **138**, 412–424 (2019).



50. Menzies, K. L. & Jones, L. The Impact of Contact Angle on the Biocompatibility of Biomaterials. *Optom. Vis. Sci.* **87**, 387 (2010).
51. Arima, Y. & Iwata, H. Effect of wettability and surface functional groups on protein adsorption and cell adhesion using well-defined mixed self-assembled monolayers. *Biomaterials* **28**(20), 3074–3082. <https://doi.org/10.1016/j.biomaterials.2007.03.013> (2007).
52. Fauchaux, N., Schweiss, R., Lützow, K., Werner, C. & Groth, T. Self-assembled monolayers with different terminating groups as model substrates for cell adhesion studies. *Biomaterials* **25**(14), 2721–2730. <https://doi.org/10.1016/j.biomaterials.2003.09.069> (2004).
53. Shamloo, A., Mohammadaliha, N., Heilshorn, S. & Bauer, A. A Comparative Study of Collagen Matrix Density Effect on Endothelial Sprout Formation Using Experimental and Computational Approaches. *Ann. Biomed. Eng.* <https://doi.org/10.1007/s10439-015-1416-2> (2015).
54. Shamloo, A., Xu, H. & Heilshorn, S. Mechanisms of vascular endothelial growth factor-induced pathfinding by endothelial sprouts in biomaterials. *Tissue Eng. A* <https://doi.org/10.1089/ten.tea.2011.0323> (2012).

## Author contributions

F. S.: Methodology, Investigation, Visualization, Formal analysis, Software, Validation, Writing—original draft. M. J.: Methodology, Investigation, Visualization, Formal analysis, Software, Validation, Writing—original draft. H. S.: Methodology, Validation, Investigation, Formal analysis, Writing—original draft. S. M.: Experimental, Writing—original draft. M.S.: Experimental A. S.: Conceptualization, Investigation, Formal analysis, Validation, Writing—review & editing, Supervision.

## Declarations

## Competing interests

The authors declare no competing interests.

## Additional information

**Supplementary Information** The online version contains supplementary material available at <https://doi.org/10.1038/s41598-025-01545-7>.

**Correspondence** and requests for materials should be addressed to A.S.

**Reprints and permissions information** is available at [www.nature.com/reprints](http://www.nature.com/reprints).

**Publisher's note** Springer Nature remains neutral with regard to jurisdictional claims in published maps and institutional affiliations.

**Open Access** This article is licensed under a Creative Commons Attribution-NonCommercial-NoDerivatives 4.0 International License, which permits any non-commercial use, sharing, distribution and reproduction in any medium or format, as long as you give appropriate credit to the original author(s) and the source, provide a link to the Creative Commons licence, and indicate if you modified the licensed material. You do not have permission under this licence to share adapted material derived from this article or parts of it. The images or other third party material in this article are included in the article's Creative Commons licence, unless indicated otherwise in a credit line to the material. If material is not included in the article's Creative Commons licence and your intended use is not permitted by statutory regulation or exceeds the permitted use, you will need to obtain permission directly from the copyright holder. To view a copy of this licence, visit <http://creativecommons.org/licenses/by-nc-nd/4.0/>.

© The Author(s) 2025